AGU PUBLICATIONS

JGR

Journal of Geophysical Research: Atmospheres

RESEARCH ARTICLE
10.1002/2017JD026868

Special Section:
Simulations of Stratospheric Sulfate Aerosol Geoengineering with the Whole Atmosphere Community Climate Model (WACCM)

This article is a companion to Mills et al. (2017), https://doi.org/10.1002/2017JD027006, Richter et al., (2017), https://doi.org/10.1002/2017JD026912, Kravitz et al. (2017), https://doi.org/10.1002/2017JD026874, and Tilmes et al. (2017), https://doi.org/10.1002/2017JD026888.

The Climate Response to Stratospheric Aerosol Geoengineering Can Be Tailored Using Multiple Injection Locations

Douglas G. MacMartin[1,2], Ben Kravitz[3], Simone Tilmes[4,5], Jadwiga H. Richter[5], Michael J. Mills[4], Jean-Francois Lamarque[4,5], Joseph J. Tribbia[5], and Francis Vitt[4]

[1]Mechanical and Aerospace Engineering, Cornell University, Ithaca, NY, USA, [2]Department of Computing and Mathematical Sciences, California Institute of Technology, Pasadena, CA, USA, [3]Atmospheric Sciences and Global Change Division, Pacific Northwest National Laboratory, Richland, WA, USA, [4]Atmospheric Chemistry, Observations, and Modeling Laboratory, National Center for Atmospheric Research, Boulder, CO, USA, [5]Climate and Global Dynamics Laboratory, National Center for Atmospheric Research, Boulder, CO, USA

Abstract By injecting different amounts of SO_2 at multiple different latitudes, the spatial pattern of aerosol optical depth (AOD) can be partially controlled. This leads to the ability to influence the climate response to geoengineering with stratospheric aerosols, providing the potential for design. We use simulations from the fully coupled whole-atmosphere chemistry climate model CESM1(WACCM) to demonstrate that by appropriately combining injection at just four different locations, 30°S, 15°S, 15°N, and 30°N, then three spatial degrees of freedom of AOD can be achieved: an approximately spatially uniform AOD distribution, the relative difference in AOD between Northern and Southern Hemispheres, and the relative AOD in high versus low latitudes. For forcing levels that yield 1–2°C cooling, the AOD and surface temperature response are sufficiently linear in this model so that the response to different combinations of injection at different latitudes can be estimated from single-latitude injection simulations; nonlinearities associated with both aerosol growth and changes to stratospheric circulation will be increasingly important at higher forcing levels. Optimized injection at multiple locations is predicted to improve compensation of CO_2-forced climate change relative to a case using only equatorial aerosol injection (which overcools the tropics relative to high latitudes). The additional degrees of freedom can be used, for example, to balance the interhemispheric temperature gradient and the equator to pole temperature gradient in addition to the global mean temperature. Further research is needed to better quantify the impacts of these strategies on changes to long-term temperature, precipitation, and other climate parameters.

Plain Language Summary Solar geoengineering, by adding aerosols to the stratosphere that reflect some sunlight, could be used to partially offset the climate change from increased carbon dioxide (CO_2). However, one of the concerns is that this does not affect the climate the same way that increased CO_2 does, leading to some regions cooling more than others. Previous simulations only injected aerosols at a single latitude. We show that if you were to inject aerosols at a combination of multiple different latitudes, you could better tailor the resulting climate response, providing a way of designing solar geoengineering to better meet climate goals. One could, for example, adjust not only the injection rate to maintain the global mean temperature at some desired value but also the temperature difference between Northern and Southern Hemispheres (which influences tropical precipitation) and the temperature difference between tropics and high-latitude regions.

Key Points:
- Injecting SO_2 at multiple latitudes allows some tailoring of the resulting climate response
- Three independent degrees of freedom of aerosol optical depth can be achieved
- Multiple injection locations may improve climate change compensation relative to equatorial injection

Correspondence to:
D. G. MacMartin,
dgm224@cornell.edu

Citation:
MacMartin, D. G., Kravitz, B., Tilmes, S., Richter, J. H., Mills, M. J., Lamarque, J.-F., Tribbia, J. J., & Vitt, F. (2017). The climate response to stratospheric aerosol geoengineering can be tailored using multiple injection locations. *Journal of Geophysical Research: Atmospheres*, *122*, 12,574–12,590. https://doi.org/10.1002/2017JD026868

Received 30 MAR 2017
Accepted 8 SEP 2017
Accepted article online 6 NOV 2017
Published online 7 DEC 2017

1. Introduction

Solar geoengineering using stratospheric aerosols has been suggested as a possible approach to reduce future impacts of climate change (e.g., Crutzen, 2006; National Academy of Sciences, 2015). One of the key questions is what the climate effects would be, including concern over differential regional effects (Kravitz et al., 2014; Ricke et al., 2010). However, one can choose not only how much aerosol to add but also where (e.g., latitude and altitude), and the choice of injection location influences the resulting climate (Tilmes et al., 2017). This motivates the need to explore the design space of stratospheric-aerosol geoengineering, and more

fundamentally, to explicitly treat geoengineering as a *design* problem, bringing an engineering perspective into research on solar geoengineering.

Simulations have typically tested specific injection scenarios, with the majority considering only equatorial injection as in the Geoengineering Model Intercomparison Project (GeoMIP) scenarios G3 and G4 (Kravitz et al., 2011; Pitari et al., 2014), and others (e.g., Aquila et al., 2014; Crook et al., 2015; Kalidindi et al., 2015; Niemeier et al., 2013; Niemeier & Timmreck, 2015). These simulations may lead to regional differences in climate outcomes, but it is unclear whether such differences are an inevitable consequence of any strategy for deploying stratospheric aerosol geoengineering or only a consequence of the specific scenario that was simulated.

The ability to optimize climate response has previously been explored only with idealized latitude-dependent solar reductions (Ban-Weiss & Caldeira, 2010; Kravitz et al., 2016; MacMartin et al., 2013). These studies all considered three independent spatial degrees of freedom: a uniform solar reduction, a reduction that varied linearly with the sine of latitude, and a quadratic variation. These correspond to the ability to separately influence the global mean temperature, the Northern versus Southern Hemisphere cooling (which influences the location of the Intertropical Convergence Zone (ITCZ) and hence tropical precipitation changes, e.g., Haywood et al., 2013), and the relative cooling between high and low latitudes. As an example, a robust result from simulations is that uniformly reducing insolation leads to less polar amplification than in the climate response to greenhouse gases, and hence undercools high latitudes relative to low (Govindasamy & Caldeira, 2000; Kravitz et al., 2013). Thus, the ability to increase how much sunlight is reflected at high latitudes relative to low, for example, can, in principle, improve the compensation for greenhouse gas climate changes, potentially reducing regional disparities in outcomes (Kravitz et al., 2016).

The three spatial degrees of freedom considered in these earlier optimization studies were motivated by what was believed to be achievable using stratospheric aerosols, based on the primarily poleward air transport of the stratospheric Brewer-Dobson circulation. Hence, injecting sufficiently far from the equator in one hemisphere is expected to predominantly increase the aerosol optical depth (AOD) in that hemisphere, while injecting further from the equator will predominantly increase AOD at higher rather than low latitudes. Indeed, Robock et al. (2008) showed, with a simpler model than used here, that Arctic and tropical SO_2 injections lead to different outcomes, with the former yielding less tropical cooling relative to Arctic cooling than the latter, although it is clear from this earlier work that energy transport within the climate system will limit what climate states can be achieved; see also MacCracken et al. (2013) and Tilmes et al. (2014).

Here we consider, for the first time, whether simultaneous injection of stratospheric SO_2 at multiple different latitudes can be used to obtain multiple independent degrees of freedom of the spatial pattern of AOD, and in turn if these lead to multiple independent degrees of freedom of the spatial pattern of surface air temperature. The amplitude and spatial pattern of AOD that results from injection at any given latitude depends on a complex interplay of factors (MacMartin et al., 2016; Pitari et al., 2016), and thus, it is not immediately clear what spatial patterns of AOD are actually achievable given the constraints imposed by stratospheric circulation, nor whether the (nonlinear) interactions between injections at different latitudes preclude useful design. Injecting SO_2 leads to sulfate aerosols through oxidation, followed by nucleation, condensation, and coagulation; these microphysical processes affect the resulting size distribution (English et al., 2012; Heckendorn et al., 2009; Pierce et al., 2010), which affects both lifetime (through sedimentation) and AOD for a given sulfate mass. The aerosols affect ozone chemistry (Solomon et al., 2016; Tilmes et al., 2008). Aerosol absorption of radiation leads to heating, affecting both the mean circulation pattern (Pitari, 1993) and variability about the mean (Aquila et al., 2014; Richter et al., 2017); these are also influenced by radiative effects from changes in ozone concentration. Heating of the tropical tropopause layer leads to increased water vapor transport into the stratosphere (Heckendorn et al., 2009; Pitari et al., 2014) that in turn influences radiative forcing (Solomon et al., 2010). All of these factors interact, and thus, to properly assess how the AOD depends on injection latitude requires a climate model that includes all of these processes: aerosol microphysics, stratospheric ozone chemistry, stratosphere-troposphere exchange, and a sufficiently well-resolved stratosphere to reasonably reproduce both the Brewer Dobson Circulation and the dominant mode of variability, the quasi-biennial oscillation (QBO). Simulations are conducted using a fully coupled chemistry climate model that includes all of these effects; the model is described briefly in section 2 and in more detail by Mills et al. (2016, 2017).

Simulations were first conducted using injection at several different latitudes and altitudes, as described by Tilmes et al. (2017), to determine how the spatial pattern of AOD and climate response depend on injection location. Results herein rely on linear superposition of the AOD and temperature response obtained from

these simulations in order to predict what would occur with some linear combination of different amounts of injection at different locations. Linearity has previously been shown to be a reasonable approximation for the climate response to different spatial patterns of solar reduction (e.g., MacMartin et al., 2013). However, there are additional physical processes involved in the response to SO_2 injection, which lead to increased nonlinearity. As the injection rate increases, some of the additional mass adds to the size of existing aerosols rather than forming new aerosols (English et al., 2012; Heckendorn et al., 2009; Niemeier & Timmreck, 2015; Pierce et al., 2010). As a result, the AOD per unit mass will decrease since larger particles are less efficient scatterers, and the total stratospheric sulfate mass may decrease due to increased gravitational sedimentation. Nonlinearities can also arise because the impact of aerosols on stratospheric circulation increases with concentration, making the spatial distribution of aerosols dependent on injection rate. Nonlinearity is evaluated for simulations of SO_2 injection at a single latitude in Tilmes et al. (2017). Before considering what can be achieved by combining injections at different latitudes, additional simulations were conducted to evaluate the extent to which simultaneous injection at different locations yields similar results to what would be predicted from simulations of injection at each location separately; these are described in section 3 and revisited in sections 4 and 5.

Section 4 demonstrates that multiple different spatial distributions of AOD are indeed achievable through choice of injection location and that these are broadly consistent with the idealized patterns of solar reduction considered in previous studies; this section also considers the temporal evolution and the seasonal dependence of the AOD. The ability to achieve multiple independent patterns of AOD enables the ability to independently influence multiple degrees of freedom of surface climate response; this is explored in section 5 to evaluate using these degrees of freedom to improve the compensation of the spatial pattern of surface air temperature change that results from increased atmospheric CO_2 concentrations.

2. Simulations

Simulations were conducted with the Community Earth System Model CESM1, with the Whole Atmosphere Community Climate Model (WACCM) as the atmospheric component, described by Mills et al. (2017). The model horizontal resolution is 0.95° in latitude by 1.25° in longitude, with 70 vertical layers extending up to 145 km altitude. The model includes prognostic aerosols using a trimodal treatment (MAM3; Liu et al., 2012), fully interactive chemistry in order to capture changes in ozone concentrations, and is coupled to ocean and land models. The model has been verified against observations for a present-day simulation (1975–2010) and has been shown to have a good representation of the observed AOD after explosive volcanic eruptions (see Mills et al., 2016, 2017 for details). This model yields an internally generated QBO without any need for nudging; this is important for capturing amplitude-dependent nonlinearities that can occur if QBO is itself influenced by the addition of aerosols as in Aquila et al. (2014). For this study, we inject SO_2, as in a variety of previous studies (e.g., Aquila et al., 2014; English et al., 2012; Heckendorn et al., 2009; Niemeier & Timmreck, 2015; Pitari et al., 2014). The detailed processes involved in the conversion of SO_2 into sulfate aerosols are represented, including oxidation to sulfuric acid, nucleation and condensation, particle growth through coagulation, and sedimentation.

An important caveat is that while the model was validated by comparison with observations of volcanic aerosol properties, there may be greater aerosol coagulation and condensation with continuous SO_2 injection than there is with impulsive volcanic eruptions, and hence the aerosol size distribution may not be as well captured by the same set of parameters of the modal aerosol model (see Mills et al., 2016 for radius and standard deviation of Aitken, accumulation, and coarse modes). While the size distribution in volcanic comparisons are largely consistent with the results of sectional models (as in English et al., 2013, Kokkola et al., 2009; Weisenstein et al., 2007), a sectional model would allow more freedom in the evolution of the size distribution for geoengineered aerosols.

At higher injection rates, it may be more effective to inject as H_2SO_4 directly (Benduhn et al., 2016; Pierce et al., 2010), as new particle formation then occurs within the high concentrations of the initial plume, leading to less condensation onto and coagulation with existing aerosols, reducing the nonlinearities arising from aerosol microphysical growth. Different aerosols will also have different scattering properties and different chemical properties (Keith et al., 2016; Weisenstein et al., 2015), leading to different effects on stratospheric dynamics and ozone for a given radiative effect. However, while the details will differ, different aerosol choices are not expected to affect the broader conclusions in this paper.

We characterize the climate response to increased greenhouse gas concentrations without geoengineering with a simulation, from 1975 through to 2100, using anthropogenic forcing from the historical period and Representative Concentration Pathway RCP8.5 (Meinshausen et al., 2011). SO_2 injection cases are branched from this RCP8.5 simulation in 2040 and simulated for 10 years. Simulations were conducted for SO_2 injection at 0° (equatorial), and at 15°, 30°, and 50° latitude in each hemisphere, at 180°E in a single grid point, and at a fixed altitude roughly 1 km and 5 km above the annual-mean tropopause height at each latitude (the actual height above the tropopause will vary seasonally). For each location, injection rates of 6, 8, and 12 Tg per year of SO_2 were simulated. These single-point injection simulations are described in detail by Tilmes et al. (2017), including the stratospheric aerosol properties and aerosol spatial distribution, the impact on radiative forcing, and some estimates of the climate response. The resulting changes in stratospheric dynamics are described by Richter et al. (2017). This paper builds on these studies to assess what can be achieved by combining injection at multiple latitudes. Here we only consider the high-altitude simulations (5 km above the annual-mean tropopause), as the spatial AOD patterns are similar for high- and low-altitude injection, but with greater AOD per unit injected mass for the high-altitude cases and also greater surface air temperature response per unit AOD. Future work could more thoroughly explore the trade-off with injection altitude and also with the time of year. Because aerosols are well mixed longitudinally, we focus on zonal-mean behavior. We also focus here on annual-mean behavior, although even with a constant rate of SO_2 injection, the resulting AOD is seasonally dependent (see section 4), which may be important in influencing changes in surface climate.

Ten year simulations are long enough to evaluate the response of stratospheric aerosol concentrations and AOD to the injection, with one caveat noted below. The aerosol concentrations increase during the first 2 years after injection starts, but the year 3 response is statistically no different from that in year 10; see Figure 1. Interannual variability in AOD is relatively small, and the stratospheric aerosol concentrations in the absence of injection are small, leading to high signal-to-noise ratio. For evaluating AOD, aerosol effective radius, and total sulfate mass, averaging over the last 8 years of each simulation gives an accurate assessment of the model response for each injection scenario with some small uncertainty due to interannual variability. Because the surface air temperature does not adjust instantaneously to changes in AOD, and the AOD does not adjust instantaneously to changes in injection, we average over the last 7 years to evaluate the expected temperature response to each injection case. The surface temperature response continues to evolve beyond 10 years, as shown in Figure 1, but the first-decade response does give useful information about how the temperature responds to forcing; section 5 discusses this limitation in more detail. Long-term changes in the tropospheric climate response will also have some influence on stratospheric circulation and hence on the spatial distribution of AOD that will not be captured in these simulations, although Figure 1 suggests that the impact of this is likely to be small. Averaging over time, each simulation thus gives us an estimate of the response pattern corresponding to a particular choice of SO_2 injection.

In addition to these single-latitude aerosol injection cases, we also consider several multiple-latitude injection cases in order to evaluate linearity; these are described next.

3. Discussion of Linearity Assumption

A first step in determining whether one can combine injections at different latitudes to achieve different outcomes is whether the response to some combination is predictable from the response to individual injection cases. If the response is linear, so that there are no significant interactions, then one can simply scale and add the responses estimated from the single-latitude simulations. This clearly will not hold exactly, but nonetheless may be a sufficiently good approximation at relevant forcing levels to project what patterns of AOD or temperature could be achieved by combining different amounts of forcing at different locations.

The spatial distribution of aerosols that results from *small-amplitude* injection will depend primarily on the baseline stratospheric circulation. However, as the injection rate increases, the aerosol size, lifetime, and spatial distribution will shift due to nonlinearities (Tilmes et al., 2017). There are two main sources of nonlinearity: higher SO_2 injection rates lead to larger aerosols and hence a reduction in AOD per unit injection, and aerosol heating and other radiative and chemical interactions will change stratospheric circulation and transport, altering the spatial distribution as the injection rate increases. Tropospheric changes due to the aerosol radiative forcing will also have some impact on stratospheric circulation.

To evaluate whether it is a reasonable approximation to predict the response to combined injection from single-latitude cases, several additional 10 year simulations were conducted with simultaneous injection at

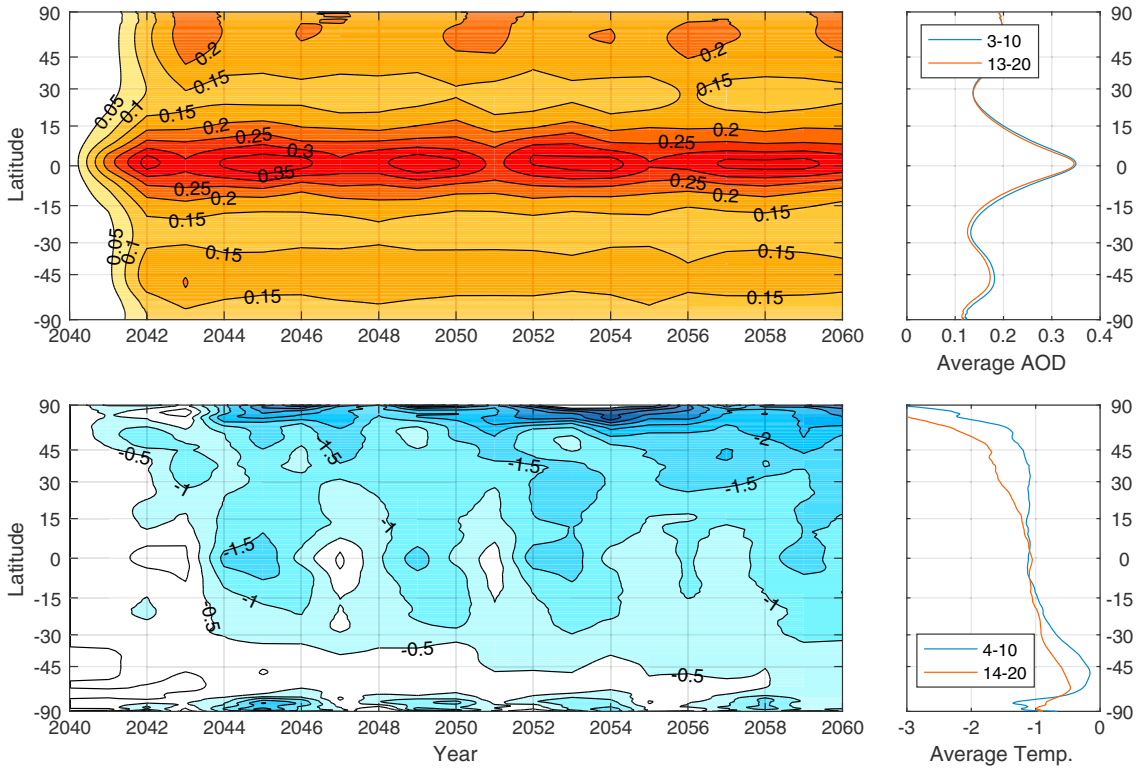

Figure 1. (top) Annual-mean aerosol optical depth and (bottom) surface air temperature resulting from equatorial SO_2 injection starting in 2040. The AOD is in steady state by year 3, but the temperature continues to evolve throughout the simulation, with the relative error most notable over the Southern Ocean. The right-hand panels show 8 year averages (for AOD) for years 3–10, used throughout this study, and years 13–20 for comparison and 7 year averages (for temperature) for years 4–10 used herein and 14–20 for comparison. All remaining simulations were conducted for only 10 years, introducing uncertainty in the estimated temperature response to SO_2 injection.

multiple latitudes to evaluate the AOD and (short-term) temperature response. A comparison between the linear prediction and actual simulation is shown for several cases in Figure 2; this figure also illustrates the zonal-mean response patterns that result from some of the single-latitude injection cases. As described by Tilmes et al. (2017), the dominant mechanism of nonlinearity is due to increased aerosol size through condensation and coagulation close to the injection point in the region of new particle formation. Figure 2 (left column) corresponds to simultaneous injection of 12 $TgSO_2$ per year each at 15°N and 15°S. When injecting only in one hemisphere, new particle formation occurs primarily in that hemisphere (Tilmes et al., 2017), and thus, there is very little interaction between the injections in each hemisphere in this case, and the total AOD is roughly the sum of the AODs from each injection separately. Figure 2 (middle column) corresponds to simultaneous injection of 12 Tg SO_2 per year each at 15°N and 30°N. In this case, the region of aerosol formation for each of these overlaps. Injecting at both locations simultaneously leads to larger aerosols than from either case alone, as evident from the effective radius. This leads to both lower SO_4 mass (due to increased sedimentation) and lower AOD per unit aerosol mass, as compared with what one would predict from the individual simulations. At these injection levels, the difference in AOD is at most roughly 20% at any latitude, with roughly a 10% difference in the global average. Nonlinear interactions may limit the applicability of the conclusions herein at sufficiently high injection rates (see also, e.g., Niemeier & Timmreck, 2015). The impact of nonlinearities on achievable patterns of AOD and surface air temperature response will be further discussed in sections 4 and 5. Figure 2 (right column) considers 6 Tg SO_2 per year at each of the four locations; from the first case considered we can expect that the Northern and Southern Hemisphere injections do not strongly interact, and so the difference between the linear sum and the actual simulation should be primarily due to the interactions between the injections in the same hemisphere and are smaller than the corresponding interactions at the higher injection rate shown in Figure 2 (middle column).

From Figure 2 we conclude that for AOD there is a reasonably linear relationship at forcing levels that result in several degrees centigrade of cooling, with the largest difference occurring at latitudes where the AOD is large.

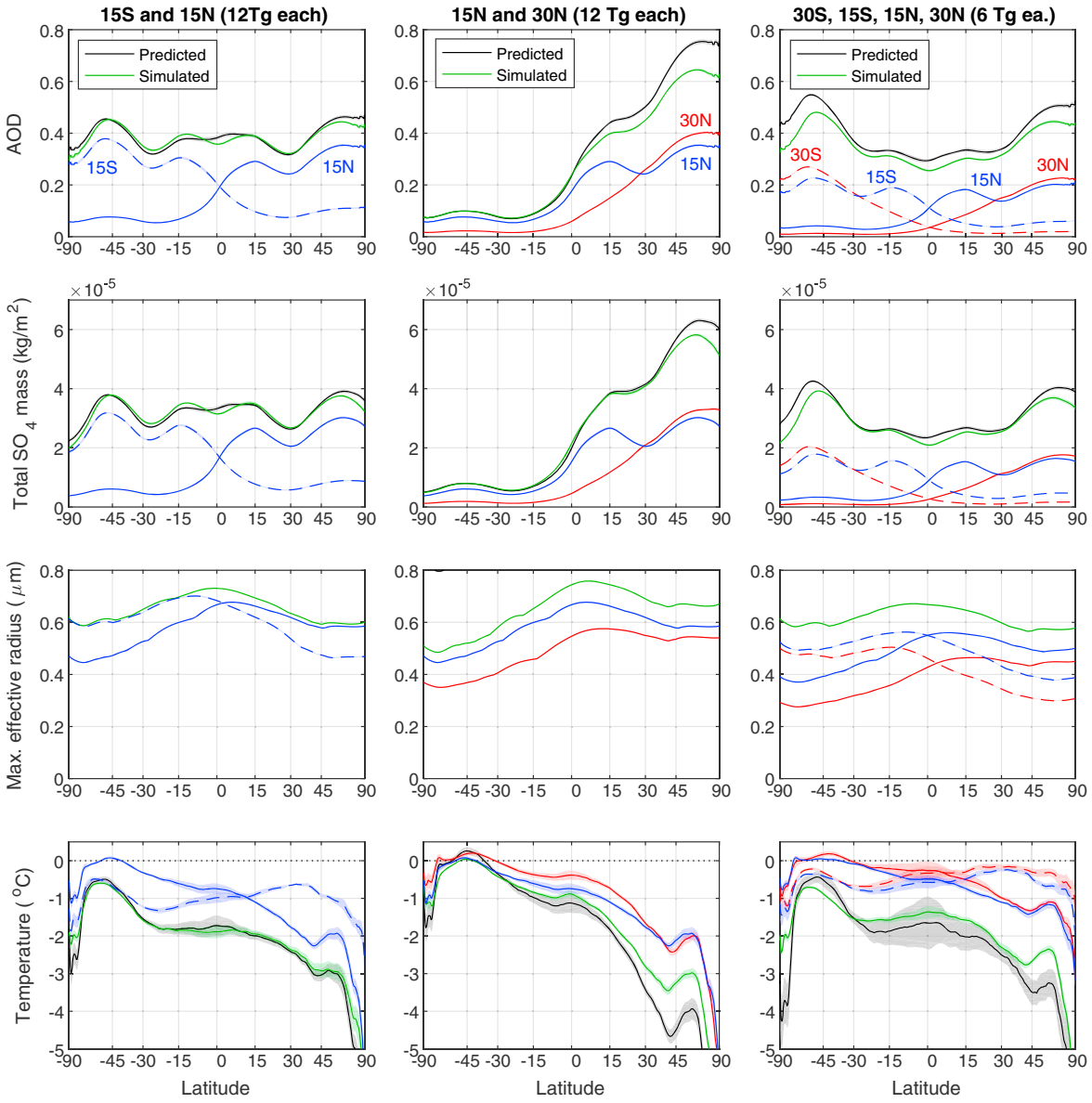

Figure 2. Response to simultaneous aerosol injection at multiple locations, compared with the response predicted from linear superposition of individual injection scenarios. (first row) Zonal-mean AOD, (second row) the stratospheric SO_4 mass burden, (third row) the maximum aerosol effective radius in the stratosphere, and (fourth row) the zonal-mean surface air temperature. Temperature responses throughout are averages over years 4–10; aerosol properties are all averages over years 3–10. Uncertainty due to natural variability is indicated with shaded bands. Cases considered are simultaneous injection at (left column) 15°S and 15°N, (middle column) 15°N and 30°N, and (right column) 30°S, 15°S, 15°N, and 30°N; the individual simulation results are shown with solid lines for Northern Hemisphere injection and dashed for Southern Hemisphere, blue for ±15° and red for ±30°. All cases are shown for a total of 24 Tg/yr injection; either 12 Tg each at two locations (left column and middle column) or 6 Tg at each of four locations (right column); this leads to roughly 2°C cooling in each case. A dominant mechanism of nonlinearity is the formation of larger aerosols, which both increases sedimentation (reducing concentrations) and results in lower AOD per unit mass.

Provided that the limitations of the linearity assumption are recognized, the spatial AOD patterns from the single-latitude aerosol injection simulations can thus be used to make reasonable projections about the AOD response that would result from different combinations of injection rates that have not been simulated; we do this in section 4. The temperature response exhibits somewhat larger nonlinearities than the stratospheric AOD. As a result of this, and also because of the relatively short simulations used here to estimate the climate response (see Figure 1), the predictions in section 5 of how well temperature changes from greenhouse gases can be compensated should be interpreted only as an initial estimate. Further work would be needed to assess the long-term temperature response.

Finally, note that it is not essential that the response be exactly linear nor perfectly known, as the injection amount could be adjusted in response to observations using a feedback process that will compensate for some amount of uncertainty or nonlinearity (Kravitz et al., 2016; MacMartin et al., 2014). Indeed, the order 20% nonlinearities noted above are sufficiently large that such a feedback process would be essential even at the injection rates considered herein unless nonlinearities could be predicted accurately in advance.

4. Achievable AOD Patterns

4.1. Optimization

By combining different rates of injection at different latitudes, what spatial patterns of AOD are possible? Given some desired spatial variation of AOD, what injection strategy best achieves it?

Previous work on geoengineering optimization and design (Ban-Weiss & Caldeira, 2010; Kravitz et al., 2016; MacMartin et al., 2013) considered three idealized spatial patterns of solar reduction denoted $L0$, for globally uniform, $L1$ for a linear variation in the sine of latitude ψ, and $L2$ for quadratic:

$$L0 = 1 \tag{1}$$

$$L1 = \sin(\psi) \tag{2}$$

$$L2 = \frac{1}{2}(3\sin^2(\psi) - 1) \tag{3}$$

For any nonnegative injection rates, the projection of the AOD onto $L1$ or half the projection onto $L2$ will be smaller than the projection onto $L0$; this provides a constraint on the space of achievable spatial distributions of AOD.

The set of injection locations we consider here are 0° (equatorial), 15°N, 15°S, 30°N, and 30°S, all at ~5 km above the annual-mean tropopause (25 km for 15° and 22 km for 30°). Injection at 50° resulted in a similar spatial pattern of AOD to injection at 30°, but with less AOD per unit injection (see Tilmes et al., 2017), and therefore did not result in additional independent degrees of freedom of the response. Different choices for injection latitude or altitude than those considered here may result in a better fit to desired AOD patterns, and additional injection locations may allow for additional spatial patterns of AOD and temperature response. For each injection latitude i, we define $\Phi_i(\psi)$ as the latitude-dependent zonal-mean pattern of AOD that results from injection at location i, estimated from the single-latitude injection simulations. The spatial pattern also depends on injection amplitude due to the nonlinearities described earlier; subsequent results use the 12 Tg SO_2 per year simulations to estimate the AOD patterns from each case unless otherwise noted. These produce of order 1°C global-mean cooling and thus might be more representative of geoengineering forcing levels than the lower rates of mass injection that were simulated. The conclusions are similar if Φ_i are estimated from 6 Tg SO_2 per year simulations instead, but with slightly lower injection rates being predicted to achieve a given result.

For any choice of desired spatial AOD pattern $G(\psi)$, then assuming linearity, the amount of injection at different latitudes that gives the best area-weighted match to that pattern can be obtained as the solution to a constrained least squares optimization problem:

$$q^* = \underset{q_i \geq 0}{\operatorname{argmin}} \left\{ \int_{-\pi/2}^{\pi/2} \left(\sum_i \Phi_i(\psi) q_i - G(\psi) \right)^2 (\cos(\psi) \mathrm{d}\psi) \right\} \tag{4}$$

where $q \in \mathbb{R}^m$ is a vector of injection amounts at each of m possible locations. The same formulation could also include different altitudes in addition to different latitudes, or different injection rates for different seasons. It would be straightforward to also include a weighting on the total amount of aerosols injected. In principle, a fit to nonlinear behavior, that is replacing $\Phi_i(\psi)q$ with the functional form $\Phi_i(\psi, q)$, could be used in a nonlinear optimization.

Figure 3 shows the result of optimizing injection amounts for fitting $L0$ (uniform), $L0 + L1$ (increasing northward), $L0 - L1$ (increasing southward), and $L0 + L2$, and gives both the fraction of the total injection to apply at each latitude and the total injection rate across all latitudes per unit average AOD (an inverse sensitivity).

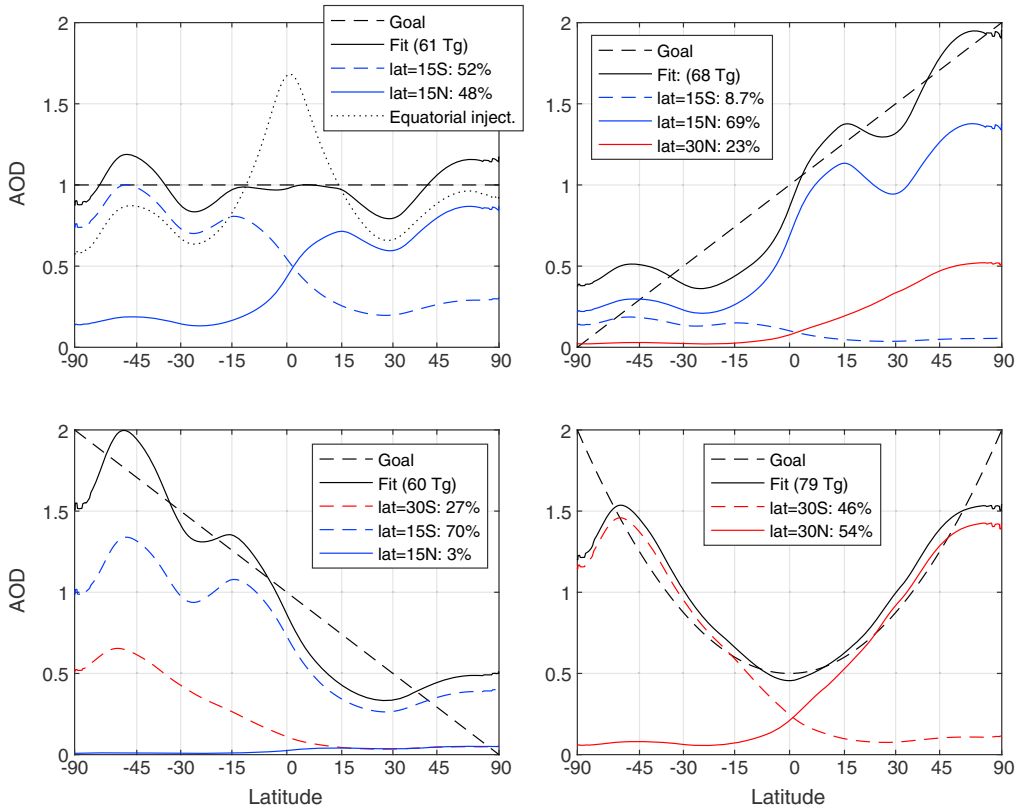

Figure 3. Combining aerosol injection at multiple locations (±15°, ±30° in latitude) to achieve different patterns of aerosol optical depth: constant (L0), linear with sine of latitude (L1) increasing either northward or southward, and quadratic (L2). For each case other than L0, the optimization goal includes an offset to ensure positive aerosol injection rates. For the L0 case, the best fit using equatorial injection is also shown (dotted line; 58 Tg/yr per unit AOD, RMS error increases from 0.09 to 0.24). The injections were performed at 25 km for equatorial, 15°N and 15°S, and 22 km for 30°N and 30°S. The fraction of injection at each latitude is shown, and the total (inverse) sensitivity in Tg/yr per unit AOD. Note that unit mean AOD is used for simplicity; the sensitivity is estimated from 12 Tg/yr injection cases and is only valid for lower values of AOD.

As these are based on linearity, quantitative estimates are only valid for smaller injection rates comparable to those used in linearity assessment in Figure 2. Note that the scaling coefficient is arbitrary; unit scaling is not a realistic value for AOD and is well beyond the range at which linearity was validated (or likely to be valid; see also Niemeier & Timmreck, 2015).

Thus, SO_2 injections at four latitudes, 30°S, 15°S, 15°N, and 30°N, enable three independent degrees of freedom of AOD. Approximately,

1. the combination of injection at 15°S and 15°N results in a global AOD pattern that is nearly constant with latitude (Figure 3, top left);
2. the combination of injection at 15°N and 30°N results in a global AOD pattern that is nearly linear (increasing northward) with the sine of latitude (Figure 3, top right);
3. the combination of injection at 15°S and 30°S results in a global AOD pattern that is nearly linear (increasing southward) with the sine of latitude (Figure 3, bottom left); and
4. the combination of injection at 30°S and 30°N results in a global AOD pattern that is nearly quadratic with the sine of latitude (Figure 3, bottom right).

None of these optimal solutions require equatorial injection, a case considered in many previous simulations of stratospheric aerosol geoengineering. The equatorial case, shown for the illustration in Figure 3 (top left) with the thin dotted line, results in a high peak in AOD in the tropics, and secondary peaks at high latitude, with a minimum AOD around 15–30° in each hemisphere. (This is similar to the spatial distribution simulated by GEOSCCM, though other model predictions differ; see Figure 3d in Pitari et al., 2014). The pattern L0–L2, providing greater emphasis on the tropics relative to the poles, is not shown in Figure 3 and cannot easily

Table 1
Projection of Zonal Mean AOD (ℓ_0, ℓ_1, ℓ_2) and Surface Air Temperature (T_0, T_1, T_2) Onto First Three Legendre Basis Functions for Various Combinations of Injection at Different Latitudes and Different Rates, Either Simulated Directly ("s") or Predicted Based On Summation of Single-Latitude Injection Cases ("p")

Injection latitude(s)	Injection rate q (Tg/yr)	Simulated or Predicted	AOD			Temperature		
			ℓ_0/q	ℓ_1/ℓ_0	ℓ_2/ℓ_0	T_0/q	T_1/T_0	T_2/T_0
15°S + 15°N	6 + 6 = 12	p	0.018	0.01	0.04	−0.103	0.64	0.47
15°S + 15°N	6 + 6 = 12	s	0.018	0.02	0.05	−0.099	0.56	0.31
15°S + 15°N	12 + 12 = 24	p	0.016	0.04	0.06	−0.087	0.70	0.45
15°S + 15°N	12 + 12 = 24	s	0.016	0.02	0.02	−0.085	0.63	0.29
15°N + 30°N	6 + 6 = 12	p	0.015	1.25	0.35	−0.098	1.44	0.75
15°N + 30°N	12 + 12 = 24	p	0.013	1.25	0.39	−0.084	1.52	0.90
15°N + 30°N	12 + 12 = 24	s	0.012	1.17	0.31	−0.067	1.37	0.77
15°S + 30°S	6 + 6 = 12	p	0.017	−1.15	0.34	−0.084	−0.24	0.37
15°S + 30°S	12 + 12 = 24	p	0.015	−1.11	0.30	−0.072	−0.23	0.19
15°S + 30°S	12 + 12 = 24	s	0.014	−1.04	0.21	−0.059	−0.25	0.01
30°S + 30°N	6 + 6 = 12	p	0.014	−0.09	0.74	−0.078	0.69	0.73
30°S + 30°N	12 + 12 = 24	p	0.013	−0.10	0.69	−0.068	0.72	0.73
30°S,15°S,15°N,30°N	4 × 6 = 24	p	0.016	−0.04	0.34	−0.091	0.66	0.58
30°S,15°S,15°N,30°N	4 × 6 = 24	s	0.015	−0.02	0.28	−0.077	0.60	0.46
0°	6	s	0.018	0.12	−0.36	−0.097	0.57	0.31
0°	12	s	0.016	0.09	−0.34	−0.077	0.64	0.17
0°	24	s	0.014	0.21	−0.27	−0.067	0.74	0.27

Note. The global-mean values ℓ_0 and T_0 are expressed per Tg/year of SO_2 injection; effectiveness decreases with injection rate and is lower for the actual simulation of some combination than for the prediction from single-injection cases. The linear and quadratic components of the response (ℓ_1, ℓ_2, and T_1, T_2) are given as ratios of the global-mean response to illustrate how the spatial pattern of AOD and temperature vary due to nonlinearities ($\ell_1 < 0$ if the linear term increases southward, $\ell_2 < 0$ if the quadratic term is higher in tropics than poles). The uncertainty in estimating ℓ_i due to natural variability is roughly 3×10^{-5} and for T_i is roughly 0.07 (so for 24 Tg/yr simulations, for example, the uncertainty in T_0/q due to natural variability is about 4%).

be achieved with the injection locations used by the optimization. The best fit to this pattern does rely on some amount of equatorial injection. However, a spatially uniform AOD is expected to overcool the tropics and undercool the poles relative to the pattern of temperature change caused by increased greenhouse gas concentrations, and thus the desired AOD pattern is likely to involve an increase toward the poles rather than a decrease. For this reason, we do not consider equatorial injection further. Also note that, in this model, high tropical aerosol concentrations that result from equatorial SO_2 injection also lead to larger aerosols (Tilmes et al., 2017), and hence, at high injection rates, equatorial injection does not yield a greater decrease in global mean temperature than other injection locations; see Table 1 described in more detail below and in section 5.

4.2. Nonlinearity Revisited

If linearity holds, then combining injections at these four latitudes would allow any positive linear combination of the spatial AOD patterns in Figure 3. An important consideration is whether the three degrees of freedom described above remain achievable given nonlinearities in the response. Table 1 shows the projection of the AOD onto the three Legendre basis functions defined in equations (1)–(3) above (ℓ_0, ℓ_1, and ℓ_2, respectively) for a number of combined-latitude cases, including those shown in Figure 2 and including both the results from the prediction made by linear superposition of single-latitude injection simulations and the result from direct simulation of a particular combination. The case of simultaneous injection at 30°S and 30°N is not expected to lead to any significant nonlinear interaction and was not directly simulated. The equatorial injection case is included for comparison; it is the only case considered in which $\ell_2 < 0$. Table 1 also includes similar results for surface air temperature that will be described in the next section. In general, higher injection rates lead to decreased global-mean AOD per Tg of injection per year, as expected, but also change the spatial pattern of AOD, as indicated by the ratio of ℓ_1 or ℓ_2 to the global-mean value ℓ_0; these ratios typically decrease. This means that the ratio of how much injection might be needed at each latitude to achieve a

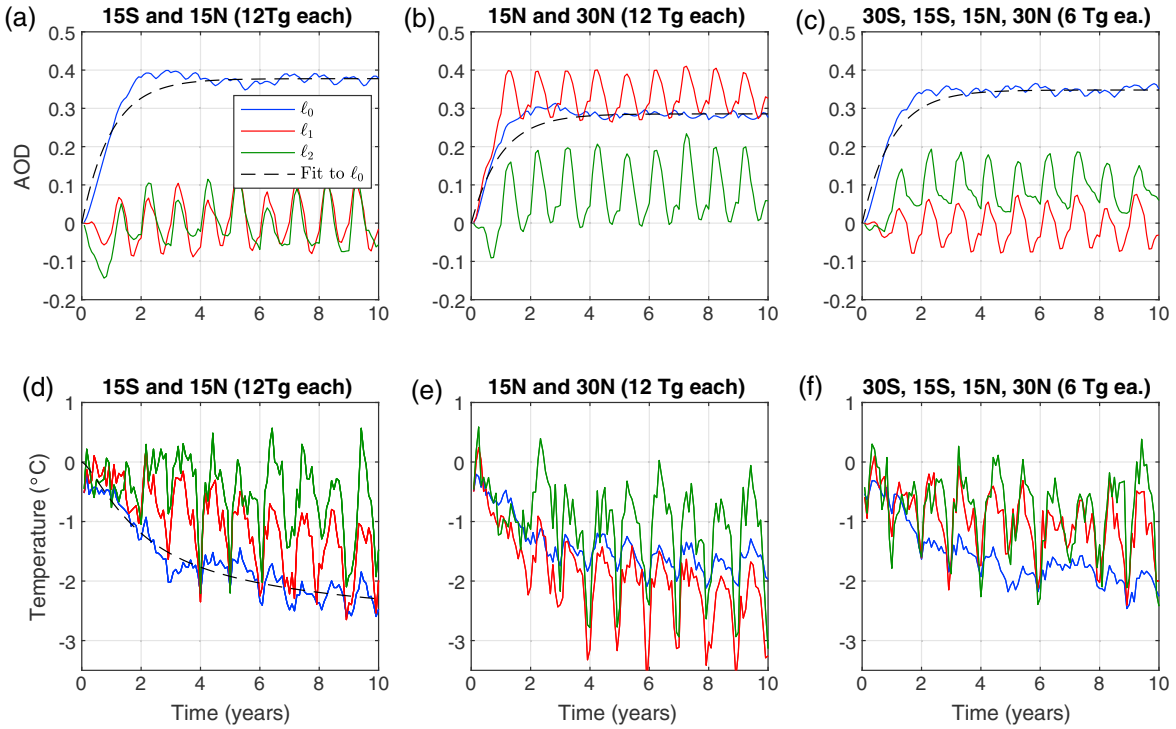

Figure 4. (a–c) Temporal evolution of the AOD response projected onto Legendre polynomials in equations (1)–(3) (ℓ_0, ℓ_1, and ℓ_2) and (d–f) surface air temperature response T_0, T_1, T_2, illustrating both the convergence (or lack thereof) of annual-mean values and the seasonal response. For the global mean AOD ℓ_0, a fit to a 1 year time constant exponential rise time is shown. For global-mean temperature T_0 in Figure 4d the fit to semiinfinite diffusion (convolved with the 1 year exponential AOD response) is shown; the steady state value from this fit is 50% larger than the average over years 4–10. Simulation cases are the same as those shown in Figure 2, including simultaneous injection of 12 Tg/yr each at 15°S and 15°N (Figures 4a and 4d), 15°N and 30°N (Figures 4b and 4e), and 6 Tg/yr each at 30°S, 15°S, 15°N, and 30°N (Figures 4c and 4f).

given combination of ℓ_0, ℓ_1, and ℓ_2 will change with the overall magnitude of AOD desired. However, despite the nonlinearities, at the injection rates considered in Table 1, it is possible to choose strategies that lead to different values for the three different coefficients ℓ_i subject to the constraint that, for example, the largest value of ℓ_1/ℓ_0 from any simulated 24 Tg/yr injection scenario is 1.17, and the largest value of ℓ_2/ℓ_0 is 0.69. It is not possible, for example, to achieve zero tropical AOD and only have nonzero AOD at high latitudes using the injection cases considered here; this would require $\ell_2/\ell_0 = 2$. (Even if this were possible, it would lead to cooling at all latitudes, not just high latitudes, due to heat transport.)

The projection onto ℓ_0, ℓ_1, and ℓ_2 also provides a useful understanding of the temporal behavior. For the same set of injection scenarios considered in Figure 2, Figures 4a–4c shows how the values of ℓ_i evolve over time, consistent with the convergence illustrated for equatorial injection in Figure 1. The AOD response to a change in injection rate is not instantaneous but has a roughly 1 year time constant. Figure 4 also illustrates the seasonal response; a seasonally constant rate of SO_2 injection does not lead to a seasonally constant spatial pattern of AOD due to the seasonal dependence of the stratospheric circulation. This again motivates future research to explore the value of seasonally varying rates of injection; Laakso et al. (2017) considers this but motivated by improving efficacy rather than altering outcomes.

4.3. Design

One additional step is required before considering the temperature response in section 5. Returning to the injection strategies shown in Figure 3, we denote the amount of injection (in Tg) at these four locations by the vector $q \in \mathbb{R}^4$, and the corresponding amount of AOD projected onto these four patterns by $\ell \in \mathbb{R}^4$,

$$q = \begin{bmatrix} q_{30S} \\ q_{15S} \\ q_{15N} \\ q_{30N} \end{bmatrix} \qquad \ell = \begin{bmatrix} \ell_0 \\ \ell_1^N \\ \ell_1^S \\ \ell_2 \end{bmatrix}$$

where $q_i \geq 0$ and $\ell_i \geq 0$, and only one of ℓ_1^N and ℓ_1^S can be nonzero. The relationships in each panel of Figure 3 can be described by $q = m_i \Rightarrow \ell = f_i$ for appropriate vectors m_i and f_i. Approximating the optimized values in Figure 3, then, for example, $q = [40\ \ 0\ \ 0\ \ 40]^T$ gives $\ell \simeq [1\ \ 0\ \ 0\ \ 1]^T$.

Assembling these columns into matrices M and F yields

$$M = \begin{bmatrix} 0 & 0 & 20 & 40 \\ 30 & 0 & 45 & 0 \\ 30 & 45 & 0 & 0 \\ 0 & 20 & 0 & 40 \end{bmatrix} \quad \text{and} \quad F = \begin{bmatrix} 1 & 1 & 1 & 1 \\ 0 & 1 & 0 & 0 \\ 0 & 0 & 1 & 0 \\ 0 & 0 & 0 & 1 \end{bmatrix}$$

For design, we would also like to be able to invert this relationship and determine how much aerosol injection we need at each location in order to achieve some specified AOD pattern; this will be used in the next section as a way of understanding how to relate the spatial response of surface air temperature to different combinations of injection at different latitudes. A desired AOD spatial pattern described by the values for its projection onto $L0$, $L1$, and $L2$ can be achieved by choosing $q = MF^{-1}\ell$, or

$$\begin{bmatrix} q_{30S} \\ q_{15S} \\ q_{15N} \\ q_{30N} \end{bmatrix} = \begin{bmatrix} 20\ell_1^S + 40\ell_2 \\ 30(\ell_0 - (\ell_1^N + \ell_1^S + \ell_2)) + 45\ell_1^S \\ 30(\ell_0 - (\ell_1^N + \ell_1^S + \ell_2)) + 45\ell_1^N \\ 20\ell_1^N + 40\ell_2 \end{bmatrix} \tag{5}$$

with q in Tg per year. Enforcing the constraints that $\ell_i \geq 0$ and $\ell_0 > (\ell_1^N + \ell_1^S + \ell_2)$ then $q_i \geq 0$, $i = 1 \ldots 4$, and again, this imposes constraints on the set of achievable spatial patterns of AOD. Also, as noted above from Table 1, the injection rates needed to achieve a given combination of ℓ_i will vary with the desired magnitude of AOD due to nonlinearities that are not accounted for in the values above that have been approximated from the 12 Tg/year injection simulations. In principle, the values in Table 1 could be used to improve these estimates if some assumptions were made regarding the functional form of nonlinearity, but as described in the next section this may not be necessary.

5. Optimizing Temperature Response

5.1. Response

The purpose of geoengineering is not to achieve given patterns of AOD, but to achieve some particular goals with respect to the climate system. One possible goal would be to avoid warming in excess of some specific target temperature. With additional spatial degrees of freedom, additional goals can also be specified, for example, to maintain the interhemispheric temperature difference, since changes in this can shift the location of the ITCZ (Haywood et al., 2013), and to maintain the temperature difference between high and low latitudes. Having defined $L0$, $L1$, and $L2$ earlier, it is natural to pose these goals as maintaining the corresponding degrees of freedom of the zonal mean surface air temperature $T(\psi)$:

$$T_0 = \frac{1}{A}\int_\psi T(\psi)\cos(\psi)\mathrm{d}\psi \tag{6}$$

$$T_1 = \frac{1}{A}\int_\psi \sin(\psi)T(\psi)\cos(\psi)\mathrm{d}\psi \tag{7}$$

$$T_2 = \frac{1}{A}\int_\psi \frac{3\sin^2(\psi) - 1}{2}T(\psi)\cos(\psi)\mathrm{d}\psi \tag{8}$$

$$\text{where} \qquad A = \int_\psi \cos(\psi)\mathrm{d}\psi \tag{9}$$

These are the temperature metrics introduced by Kravitz et al. (2016). Note that with only N degrees of freedom available, then only N independent climate variables (or combinations thereof) can be simultaneously managed.

Different spatial patterns of AOD do not directly map onto correspondingly different spatial patterns of temperature, as discussed by Tilmes et al. (2017). First, the radiative forcing does not have the same spatial pattern as AOD, both due to the spatial dependence of insolation and due to changes in cloud patterns and surface

albedo (e.g., Figure 10 in Tilmes et al., 2017). And second, the temperature response does not have the same spatial pattern as the radiative forcing due to differences in local feedback strengths as well as changes in heat transport. Table 1, discussed earlier, also shows the temperature as described by T_0, T_1, and T_2; it is clear that even if ℓ_1 is small (e.g., injection at 15°N and 15°S), then T_1 is not small (as is also true for CO_2 warming) and that if ℓ_2 is small, T_2 is not (due to polar amplification). Further, while the response is nonlinear, a similar conclusion holds here as for AOD: different choices of injection location yield different values for the spatial pattern of temperature even in the presence of all of the other processes that influence the response to forcing. Again, there will be limits on what can be achieved: for example, using these aerosol injection latitudes one cannot cool the Arctic without also cooling the tropics, but there is nonetheless some ability to influence the relative cooling between high and low latitudes through the choice of injection locations. As with AOD, nonlinearities affect the relationship between injection and response.

The evolution of T_0, T_1,and T_2 with time are shown in Figures 4d–4f for the same simulation cases shown in Figures 2. The response of the global-mean temperature T_0 to relatively spatially uniform forcing due to either CO_2 or solar forcing has previously been shown to be well approximated by a semiinfinite diffusion model; see, for example, Caldeira and Myhrvold (2013) and MacMynowski et al. (2011), respectively. A fit to this behavior (coupled with the 1 year exponential response of the AOD to injection) is included, from which one could infer that the average response over years 4–10 might underpredict the long-term response by 50%. However, there is no basis to justify using a similar functional form to extrapolate the response to the spatially nonuniform forcing here that allows some ability to independently influence T_0, T_1, and T_2. For this reason, the fit is only shown for the response to simultaneous injection at 15°S and 15°N. As for the AOD, Figures 4d–4f also illustrate that the response pattern will vary seasonally. While the analysis below describes the estimated changes in annual-mean temperature behavior, differences between the seasonal dependence of greenhouse gas induced warming and stratospheric aerosol cooling are likely to be important, particularly at higher latitudes where both the AOD and the insolation exhibit strong seasonality.

If the AOD corresponding to each pattern ℓ is obtained from multiple-latitude injections using the relationship $q = MF^{-1}\ell$ determined in section 4 above, then the temperature response that would result from each pattern of aerosol injection can be estimated based on the corresponding linear combination of the temperature responses obtained from the single-latitude injection simulations. These are based on the average response over the last 7 years of a 10 year simulation, and thus will underestimate the equilibrium response, as noted above. With these caveats in mind, the best estimate of the system input-output response, shown in Figure 5, is

$$\begin{bmatrix} T_0 \\ 3T_1 \\ 5T_2 \end{bmatrix} \simeq \begin{bmatrix} \mathbf{-5.2} & \mathit{-0.4} & \mathit{0.3} & \mathit{-0.2} \\ -3.7 & \mathbf{-4.4} & \mathbf{4.3} & \mathit{-0.2} \\ -2.4 & -2.2 & 1.5 & \mathbf{-1.6} \end{bmatrix} \begin{bmatrix} \ell_0 \\ \ell_1^N \\ \ell_1^S \\ \ell_2 \end{bmatrix} \tag{10}$$

Perturbations in ℓ_0 affect T_0, T_1, and T_2. Perturbations in ℓ_1 (of either sign) primarily affect T_1 and T_2, with much smaller impact on T_0 than perturbations in ℓ_0 have. Perturbations in ℓ_2 primarily influence only T_2, with again much smaller influence on T_0 and T_1 than ℓ_0 or ℓ_1 have. The relationship is thus mostly lower triangular; the "diagonal" elements above are shown in **bold** and the relatively smaller upper triangular elements in *italics*. Because each of these three patterns of AOD affects surface air temperature differently, then three degrees of freedom of surface air temperature can be independently chosen by choosing the pattern of AOD, and hence injection amounts at different latitudes (subject to the constraint that injection amounts must be positive).

The relationships in equation (10) are ultimately why we started by considering achievable patterns of AOD. One could rewrite equation (10) to explicitly relate the temperature pattern directly in terms of injection rates at each location. However, the input/output response would then be fully coupled. Relating injection rates at each location to achievable patterns of AOD allows us to express the relationship between temperature and AOD through this partially decoupled structure, which in turn enables a constructive algorithm to solve for the injection rates to achieve a desired temperature, described below.

5.2. Optimization

We now consider whether allowing aerosol injection at multiple locations simultaneously can improve the compensation of anthropogenic climate change. To capture the spatial pattern of temperature change from greenhouse gases, we take the difference over 50 years, between the decades 2065–2074 and 2015–2024 for

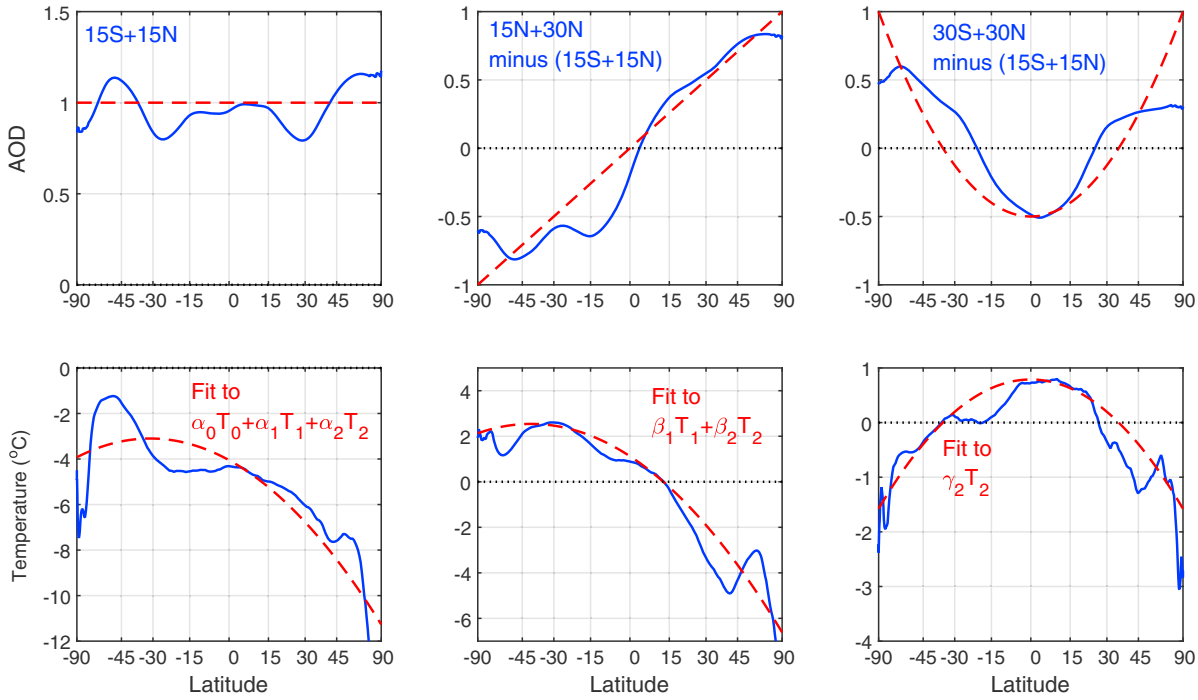

Figure 5. Relationship between different patterns of AOD and surface air temperature, leading to an overall design strategy. The second and third cases (L1 and L2) correspond to subtracting the nearly uniform AOD that results from 15°N and 15°S injection from the relevant cases shown in Figure 3 in order to obtain a zero-mean AOD pattern (not realizable by themselves, but realizable in combination with the first pattern of AOD; this is simply a convenient change of basis). Each pattern of AOD results in a different pattern of temperature, allowing three degrees of freedom of temperature to be independently chosen.

the RCP8.5 control simulation and scale this to a global-mean warming of 1°C. This gives us the zonal-mean pattern of warming shown in Figure 6a, black line. (The modeled global mean temperature change over the 50 years is nearly 3°C, beyond the range at which we evaluated linearity in section 3; at high forcing levels, efficacy per unit forcing decreases.)

Optimizing the amount of injection at each latitude could either be done directly as in equation (4) or by projecting the desired spatial pattern of cooling onto $L0$, $L1$, and $L2$, solving for the required spatial pattern of AOD using equation (10), and then solving for the injection amounts needed to achieve that pattern using equation (5). Either approach yields similar results. We choose to solve for the injection amounts using the latter approach as this two-step process provides a pathway toward a feedback algorithm that can adjust the injection amounts each year in response to differences between desired and simulated outcomes.

Given some desired change in surface air temperature described by its projections T_0, T_1, and T_2 onto $L0$, $L1$, and $L2$, equations (10) and (5) lead to a constructive algorithm for finding the injection rates needed to achieve this pattern. The value of ℓ_0, the desired projection of the AOD onto $L0$, is chosen to compensate for T_0. Next, the projection ℓ_1 onto $L1$ is chosen to compensate for the combination of T_1 and the effect of ℓ_0 on T_1, and the constraint $|\ell_1| \leq \ell_0$ enforced. This constraint limits the range of values of T_1 that can be achieved for a given choice of T_0. The projection ℓ_2 onto $L2$ can then be chosen to compensate for the original desired value T_2, and the combined effect of ℓ_0 and ℓ_1 on T_2, with the constraint $\ell_2 \leq \ell_0 - |\ell_1|$ enforced, similarly limiting the achievable range of T_2. Note that enforcing the constraints in this order ensures that priority is placed on meeting the global mean temperature, then the interhemispheric gradient T_1, and then the equator to pole gradient T_2. Finally, the injection rates q_i can be chosen from equation (5). Because of uncertainties and nonlinearities, this solution will not achieve the desired temperature distribution. (This would be true even if the matrix M had not been approximated.) However, this forms the basis for an iterative feedback algorithm that will converge to the desired values. Given the error between desired and actual temperatures, one can use the approach described above to move in the right direction, observe the new error, make a new correction, and so forth.

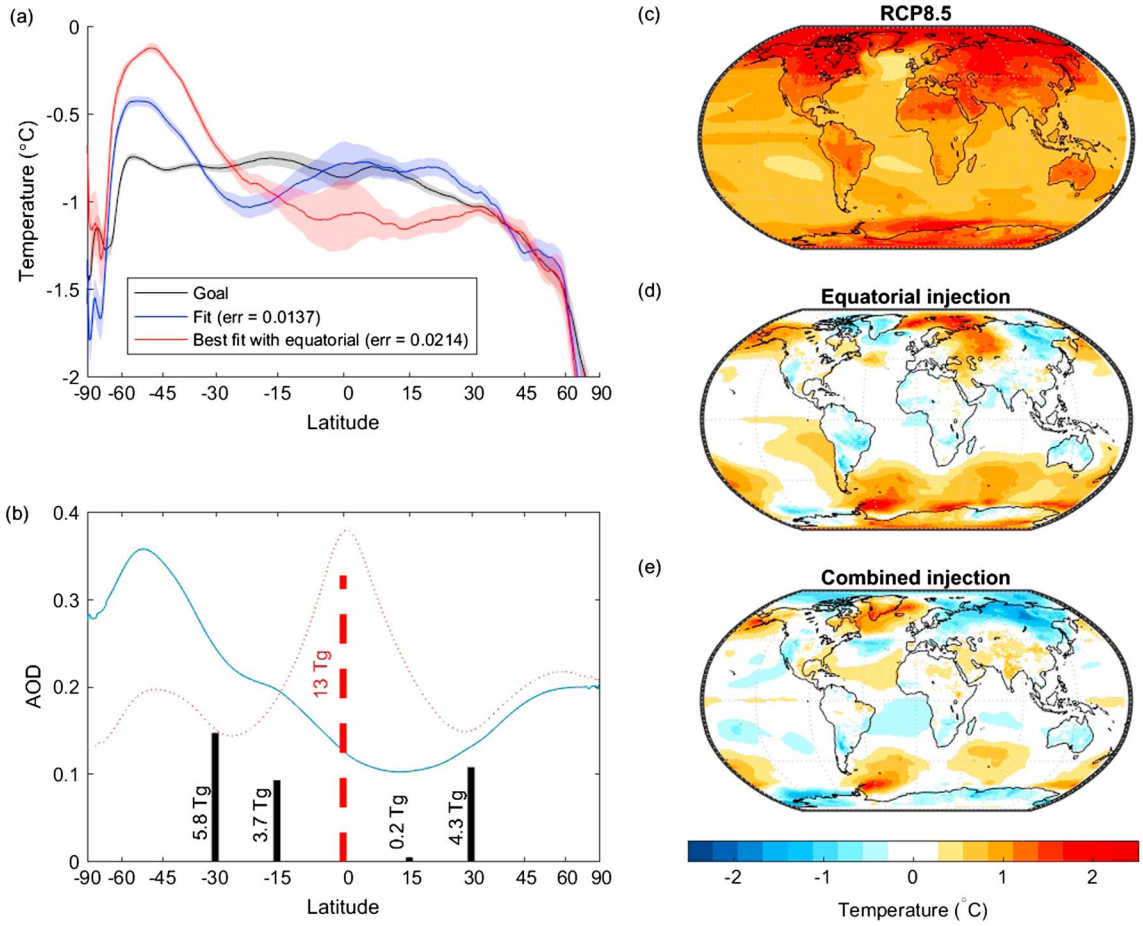

Figure 6. Combining aerosol injection at multiple locations (±15°, ±30° in latitude) to compensate for the zonal-mean temperature pattern due to increased greenhouse gases. The "goal" is shown by the black curve in Figure 6a; this is the cooling required to compensate for the zonal-mean pattern of warming, scaled to 1°C global-mean temperature change. (a) The best fit to this temperature reduction using either four injection locations or only equatorial injection; the former corrects for the projection onto global-mean (T_0), interhemispheric gradient (T_1), and equator to pole gradient (T_2), while the equatorial injection only compensates for T_0. Shaded bands indicate uncertainty in the patterns due only to natural variability (not due to nonlinearity or due to the short simulations used in estimating responses). (b) The corresponding projected AOD; thick vertical lines indicate the amount of injection used at each latitude in the multilatitude solution (black, 14 Tg total) and the equatorial injection case (13 Tg). (c–e) The projected temperature change without geoengineering (1°C mean), and the residual temperature responses due to either equatorial injection alone or the optimized combination of injection at multiple latitudes (both 0°C mean). The area-weighted mean square error in compensating temperature is reduced from 19% to 13%.

In subsequent work that builds on the results herein, Kravitz et al. (2017) adjust SO_2 mass injection rates at these four latitudes to simultaneously manage multiple degrees of freedom of the zonal-mean surface air temperature response, using the same basic feedback strategy but with a slightly more complicated proportional integral controller as described by MacMartin et al. (2014) and Kravitz et al. (2016).

The best achievable pattern of cooling is given by the blue line in Figure 6a, and the red line shows the corresponding compensation using only equatorial aerosol injection to balance only the global-mean temperature response. As expected, using only equatorial injection overcools the tropics relative to higher latitudes. Including the ability to compensate for T_1 has a relatively minor impact on the solution: while $T_1 > 0$ even for choices that lead to $\ell_1 = 0$ (Table 1, Figure 5, or equation (10)), this is also true for greenhouse gas warming due to the higher land area in the Northern Hemisphere. However, there is a substantial improvement by providing the ability to compensate for T_2 by putting more of the mass injection at higher latitudes, because the polar amplification of warming due to greenhouse gases alone is stronger than the polar amplification of warming due to a spatially uniform AOD ($\ell_1 = \ell_2 = 0$). The spatial AOD patterns corresponding to the equatorial-only and the multiple-latitude solution (calculated from linear superposition of the single-point injection simulations) are shown in Figure 6b. Figures 6c–6e illustrate the projected temperature compensation globally. The area-weighted mean square temperature differences are reduced by 30% in this analysis.

The pattern of temperature response in a multidecadal simulation using these injection amounts would differ from that predicted here, both because the influence functions here are determined from only 10 year simulations and because of the nonlinearities discussed earlier. In particular, Figure 1 makes it clear that the substantial undercooling over the Southern Ocean in Figure 6 is at least in part a result of a longer time constant for warming and thus is a limitation of using short simulations to estimate the climate response. These projections should only be considered as estimates of what may be achievable with multiple injection locations. However, a feedback approach, wherein the amount of injection at each location is adjusted in response to the observed rather than predicted changes, could compensate for the uncertainty and nonlinearity in both the magnitude and the spatial pattern of the long-term temperature response. This could be used not only in climate model simulations, but possibly in any future deployment and would avoid the need to perfectly characterize either nonlinearities or long-term responses. Thus, while these caveats suggest caution on quantitative estimates, these predictions suggest that using multiple aerosol injection locations could yield notably improved compensation of the greenhouse gas warming than stratospheric aerosol geoengineering with only single-point injection (Figure 6d and dashed red line in Figure 6a).

6. Conclusions

An important question to address regarding solar geoengineering with stratospheric aerosols is the best estimate for the projected climate effects. The climate effects depend on the spatial distribution of aerosols within the stratosphere, which is at least partially a design choice enabled by choosing how much mass to inject at multiple different latitudes. Thus the question regarding projected climate effects cannot be fully answered without treating geoengineering as a design problem.

Using a climate model that includes many of the essential processes that influence the spatial distribution of aerosol optical depth, we demonstrate for the first time that combining different amounts of SO_2 injection at four different latitudes allows multiple independent spatial patterns of aerosol optical depth to be achieved, although the constraints imposed by stratospheric circulation means that the pattern of AOD cannot be specified arbitrarily. The stratospheric Brewer-Dobson circulation predominantly transports aerosols poleward; it is thus straightforward both to inject sufficiently far from the equator to preferentially yield an increased aerosol burden in only one or the other hemisphere or to preferentially increase the aerosol burden at higher rather than lower latitudes. As a result, four injection locations are sufficient to approximately achieve three independent spatial degrees of freedom of response: a spatially uniform AOD, an AOD that varies with the sine of latitude either northward or southward, and an AOD that varies quadratically with the sine of latitude. Because each of the spatial patterns of AOD obtained here result in different patterns of surface air temperature response, then three degrees of freedom of the temperature response can be independently managed by choosing how much to inject at each latitude; the achievable response is subject to constraints imposed both by the stratospheric circulation limiting achievable AOD patterns and by climate processes that affect the response to forcing. Nonetheless, this has the potential to improve how well geoengineering can compensate for anthropogenic climate change. The potential for this *design* aspect should be taken into account before assessing expected climate impacts from solar geoengineering.

A more comprehensive survey of injection latitudes may lead to an improved match of the degrees of freedom considered herein and may identify additional degrees of freedom that can be attained. It may also be possible to alter the response by other strategies such as modulating the injection amount seasonally, taking advantage of the seasonal dependence of the stratospheric circulation to achieve additional spatial AOD patterns.

It is important to note that the spatial distribution of aerosols resulting from a given injection strategy depends on the stratospheric circulation and a complex interplay of aerosol microphysics, chemistry, and radiative changes in both the mean stratospheric circulation and modes of variability. The results obtained herein are based on simulations with CESM1(WACCM) that include all of these elements. An important caveat is that these model simulations use fixed mode widths in a modal aerosol treatment rather than a more computationally intensive sectional model; while the parameters of the modal model yield aerosol size distributions that have been validated with observations from volcanic eruptions, the size and hence spatial distribution for geoengineered aerosols may differ. The response to injection is also not linear: injecting at multiple latitudes simultaneously results in interactions and a response different from the linear superposition of the responses to injection at each latitude separately. The dominant nonlinearity is due to aerosol growth in regions of high

SO_2 concentrations (Tilmes et al., 2017); it may be possible to reduce this nonlinearity through different injection strategies (Pierce et al., 2010). Nonetheless, even at forcing levels sufficient to offset 1–2°C of warming, the response to SO_2 injection is sufficiently close to linear in this model so that predictions based off a linear assumption remain useful.

All of the results herein are from a model, and the real world will behave differently. Nonetheless, the results are physically motivated and the broad conclusions can be reasonably expected to remain valid. Specific results shown here for temperature compensation in particular should be interpreted cautiously in part because of the short (10 year) simulations used here. This choice was determined by computational considerations and while sufficient to make reasonable projections of AOD response, are insufficient for accurately estimating either the magnitude or spatial pattern of long-term temperature projections. Uncertainty and nonlinearity in the relationship between injection and response could be compensated in model simulations or a hypothetical future deployment using feedback of the "observed" response to adjust injection amounts.

Acknowledgments
Albert Chu at Cornell assisted in generating the fit in Figure 4d. The CESM project is supported by the National Science Foundation and the Office of Science (BER) of the U.S. Department of Energy. The National Center for Atmospheric Research is sponsored by the National Science Foundation. The Pacific Northwest National Laboratory is operated for the U.S. Department of Energy by Battelle Memorial Institute under contract DE-AC05-76RL01830. Computing resources were provided by the Climate Simulation Laboratory at NCAR's Computational and Information Systems Laboratory (CISL) (Computational and Information Systems Laboratory, 2012), sponsored by the National Science Foundation and other agencies with high-performance computing support from Yellowstone (ark:/85065/d7wd3xhc). This research was developed with funding from the Defense Advanced Research Projects Agency (DARPA). The views, opinions, and/or findings expressed are those of the authors and should not be interpreted as representing the official views or policies of the Department of Defense or the U.S. Government. Simulation output are available at https://www.earthsystemgrid.org/dataset/ucar.cgd.ccsm4.so2_geoeng.html.

References

Aquila, V., Garfinkel, C. I., Newman, P. A., Oman, L. D., & Waugh, D. W. (2014). Modifications of the quasi-biennial oscillation by a geoengineering perturbation of the stratospheric aerosol layer. *Geophysical Research Letters*, *41*, 1738–1744. https://doi.org/10.1002/2013GL058818

Ban-Weiss, G. A., & Caldeira, K. (2010). Geoengineering as an optimization problem. *Environmental Research Letters*, *5*, 34009. https://doi.org/10.1088/1748-9326/5/3/034009

Benduhn, F., Schallock, J., & Lawrence, M. G. (2016). Early growth dynamical implications for the steerability of stratospheric solar radiation management via sulfur aerosol particles. *Geophysical Research Letters*, *43*, 9956–9963. https://doi.org/10.1002/2016GL070701

Caldeira, K., & Myhrvold, N. (2013). Projections of the pace of warming following an abrupt increase in atmospheric carbon dioxide concentration. *Environmental Research Letters*, *8*, 34039.

Computational and Information Systems Laboratory (2012). Yellowstone: IBM iDataPlex System (NCAR Strategic Capability Projects), Boulder, CO: National Center for Atmospheric Research. https://n2t.net/ark:/85065/d7wd3xhc

Crook, J. A., Jackson, L. S., Osprey, S. M., & Forster, P. M. (2015). A comparison of temperature and precipitation responses to different Earth radiation management geoengineering schemes. *Journal of Geophysical Research: Atmospheres*, *120*, 9352–9373. https://doi.org/10.1002/2015JD023269

Crutzen, P. J. (2006). Albedo enhancement by stratospheric sulfur injections: A contribution to resolve a policy dilemma? *Climatic Change*, *77*, 211–219. https://doi.org/10.1007/s10584-006-9101-y

English, J. M., Toon, O. B., & Mills, M. J. (2012). Microphysical simulations of sulfur burdens from stratospheric sulfur geoengineering. *Atmospheric Chemistry and Physics*, *12*(10), 4775–4793.

English, J. M., Toon, O. B., & Mills, M. J. (2013). Microphysical simulations of large volcanic eruptions: Pinatubo and Toba. *Journal of Geophysical Research: Atmospheres*, *118*, 1880–1895. https://doi.org/10.1002/jgrd.50196

Govindasamy, B., & Caldeira, K. (2000). Geoengineering Earth's radiation balance to mitigate CO_2-induced climate change. *Geophysical Research Letters*, *27*, 2141–2144. https://doi.org/10.1029/1999GL006086

Haywood, J. M., Jones, A., Bellouin, N., & Stephenson, D. (2013). Asymmetric forcing from stratospheric aerosols impacts Sahelian rainfall. *Nature Climate Change*, *3*, 660–665. https://doi.org/10.1038/nclimate1857

Heckendorn, P., Weisenstein, D., Fueglistaler, S., Luo, B. P., Rozanov, E., Schraner, M., … Peter, T. (2009). The impact of geoengineering aerosols on stratospheric temperature and ozone. *Environmental Research Letters*, *4*(4), 45108.

Kalidindi, S., Bala, G., Modak, A., & Caldeira, K. (2015). Modeling of solar radiation management: A comparison of simulations using reduced solar constant and stratospheric sulphate aerosols. *Climate Dynamics*, *44*(9), 2909–2925. https://doi.org/10.1007/s00382-014-2240-3

Keith, D. W., Weisenstein, K. K., Dykema, J. A., & Keutsch, F. N. (2016). Stratospheric solar geoengineering without ozone loss? *Proceedings of the National Academy of Sciences*, *113*(52), 14,910–14,914.

Kokkola, H., Hommel, R., Kazil, J., Niemeier, U., Partanen, A.-I., Feichter, J., & Timmreck, C. (2009). Aerosl microphysics modules in the framework of the ECHAM5 climate model—Intercomparison under stratospheric conditions. *Geoscientific Model Development*, *2*, 97–112. https://doi.org/10.5194/gmd-2-97-2009

Kravitz, B., Robock, A., Boucher, O., Schmidt, H., Taylor, K. E., Stenchikov, G., & Schulz, M. (2011). The Geoengineering Model Intercomparison Project (GeoMIP). *Atmospheric Science Letters*, *12*, 162–167. https://doi.org/10.1002/asl.316

Kravitz, B., Caldeira, K., Boucher, O., Robock, A., Rasch, P. J., Alterskjær, K., … Yoon, J.-H. (2013). Climate model response from the Geoengineering Model Intercomparison Project (GeoMIP). *Journal of Geophysical Research: Atmospheres*, *118*, 8320–8332. https://doi.org/10.1002/jgrd.50646

Kravitz, B., MacMartin, D. G., Robock, A., Rasch, P. J., Ricke, K. L., Cole, J. N. S., … Yoon, J.-H. (2014). A multi-model assessment of regional climate disparities caused by solar geoengineering. *Environmental Research Letters*, *9*(7), 74013. https://doi.org/10.1088/1748-9326/9/7/074013

Kravitz, B., MacMartin, D. G., Wang, H., & Rasch, P. J. (2016). Geoengineering as a design problem. *Earth Systems Dynamics*, *7*, 469–497. https://doi.org/10.5194/esd-7-469-2016

Kravitz, B., MacMartin, D. G., Mills, M. J., Richter, J. H., Tilmes, S., Lamarque, J.-F., … Vitt, F. (2017). First simulations of designing stratospheric sulfate aerosol geoengineering to meet multiple simultaneous climate objectives. *Journal of Geophysical Research: Atmospheres*, *122*. https://doi.org/10.1002/2017JD026874

Laakso, A., Korhonen, H., Romakkaniemi, S., & Kokkola, H. (2017). Radiative and climate effects of stratospheric sulfur geoengineering using seasonally varying injection areas. *Atmospheric Chemistry and Physics*, *17*, 6957–6974. https://doi.org/10.5194/acp-17-6957-2017

Liu, X., Easter, R. C., Ghan, S. J., Zaveri, R., Rasch, P., Shi, X., … Mitchell, D. (2012). Toward a minimal representation of aerosols in climate models: Description and evaluation in the Community Atmosphere Model CAM5. *Geoscientific Model Development*, *5*(3), 709–739. https://doi.org/10.5194/gmd-5-709-2012

MacCracken, M. C., Shin, H.-J., Caldeira, K., & Ban-Weiss, G. A. (2013). Climate response to imposed solar radiation reductions in high latitudes. *Earth System Dynamics*, *4*, 301–315. https://doi.org/10.5194/esd-4-301-2013

MacMartin, D. G., Keith, D. W., Kravitz, B., & Caldeira, K. (2013). Management of trade-offs in geoengineering through optimal choice of non-uniform radiative forcing. *Nature Climate Change*, *3*, 365–368. https://doi.org/10.1038/nclimate1722

MacMartin, D. G., Kravitz, B., Keith, D. W., & Jarvis, A. J. (2014). Dynamics of the coupled human-climate system resulting from closed-loop control of solar geoengineering. *Climate Dynamics*, *43*(1–2), 243–258. https://doi.org/10.1007/s00382-013-1822-9

MacMartin, D. G., Kravitz, B., Long, J. C. S., & Rasch, P. J. (2016). Geoengineering with stratospheric aerosols: What don't we know after a decade of research?. *Earth's Future*, *4*, 543–548. https://doi.org/10.1002/2016EF000418

MacMynowski, D. G., Shin, H.-J., & Caldeira, K. (2011). The frequency response of temperature and precipitation in a climate model. *Geophysical Research Letters*, *38*, L16711. https://doi.org/10.1029/2011GL048623

Meinshausen, M., Smith, S. J., Calvin, K. V., Daniel, J. S., Kainuma, M. L. T., Lamarque, J.-F., … van Vuuren, D. (2011). The RCP greenhouse gas concentrations and their extension from 1765 to 2300. *Climatic Change*, *109*, 213–241. https://doi.org/10.1007/s10584-011-0156-z

Mills, M., Richter, J. H., Tilmes, S., Kravitz, B., MacMartin, D., Glanville, S., … Lamarque, J.-F. (2017). Radiative and chemical response to interactive stratospheric aerosols in fully coupled CESM1(WACCM). *Journal of Geophysical Research: Atmospheres*, *122*. https://doi.org/10.1002/2017JD027006

Mills, M. J., Schmidt, A., Easter, R., Solomon, S., Kinnison, D. E., Ghan, S. J., … Gettelman, A. (2016). Global volcanic aerosol properties derived from emissions, 1990–2014, using CESM1(WACCM). *Journal of Geophysical Research: Atmospheres*, *121*, 2332–2348. https://doi.org/10.1175/JCLI-D-12-00558.1

National Academy of Sciences (2015). *Climate intervention: reflecting sunlight to cool Earth*. Washington DC: The National Academies Press.

Niemeier, U., & Timmreck, C. (2015). What is the limit of climate engineering by stratospheric injection of SO_2? *Atmos Chemical Physics*, *15*, 9129–9141.

Niemeier, U., Schmidt, H., Alterskjær, K., & Kristjánsson, J. E. (2013). Solar irradiance reduction via climate engineering: Impact of different techniques on the energy balance and the hydrological cycle. *Journal of Geophysical Research: Atmospheres*, *118*, 11,905–11,917. https://doi.org/10.1002/2013JD020445

Pierce, J. R., Weisenstein, D. K., Heckendorn, P., Peter, T., & Keith, D. W. (2010). Efficient formation of stratospheric aerosol for climate engineering by emission of condensible vapor from aircraft. *Geophys Research Letters*, *37*, L18805. https://doi.org/10.1029/2010GL043975

Pitari, G. (1993). A numerical study of the possible perturbation of stratospheric dynamics due to Pinatubo aerosols: Implications for tracer transport. *Journal of the Atmospheric Sciences*, *50*, 2443–2461.

Pitari, G., Aquila, V., Kravitz, B., Robock, A., Watanabe, S., Cionni, I., … Tilmes, S. (2014). Stratospheric ozone response to sulfate geoengineering: Results from the Geoengineering Model Intercomparison Project (GeoMIP). *Journal of Geophysical Research: Atmospheres*, *119*, 2629–2653. https://doi.org/10.1002/2013JD020566

Pitari, G., Genova, G. D., Mancini, E., Visioni, D., Gandolfini, I., & Cionni, I. (2016). Stratospheric aerosols from major volcanic eruptions: A composition-climate model study of the aerosol cloud dispersal and *e*-folding time. *Atmosphere*, *7*(6), 75. https://doi.org/10.3390/atmos7060075

Richter, J. H., Tilmes, S., Mills, M. J., Tribbia, J. J., Kravitz, B., Vitt, F., & Lamarque, J.-F. (2017). Stratospheric dynamical response and ozone feedbacks in the presence of SO_2 injection. *Journal of Geophysical Research: Atmospheres*, *122*. https://doi.org/10.1002/2017JD026912

Ricke, K. L., Granger Morgan, M., & Allen, M. R. (2010). Regional climate response to solar-radiation management. *Nature Geoscience*, *3*, 537–541.

Robock, A., Oman, L., & Stenchikov, G. (2008). Regional climate responses to geoengineering with tropical and Arctic SO_2 injections. *Journal of Geophysical Research*, *113*, D16101. https://doi.org/10.1029/2008JD010050

Solomon, S., Rosenlof, K. H., Portmann, R. W., Daniel, J. S., Davis, S. M., Sanford, T. J., & Plattner, G.-K. (2010). Contributions of stratospheric water vapor to decadal changes in the rate of global warming. *Science*, *327*(5970), 1219–1223.

Solomon, S., Ivy, D. J., Kinnison, D. E., Mills, M. J., Neely III, R. R., & Schmidt, A. (2016). Emergence of healing in the Antarctic ozone layer. *Science*, *353*, 269–274.

Tilmes, S., Müller, R., & Salawitch, R. (2008). The sensitivity of polar ozone depletion to proposed geoengineering schemes. *Science*, *320*(5880), 1201–1204. https://doi.org/10.1126/science.1153966

Tilmes, S., Jahn, A., Kay, J. E., Holland, M., & Lamarque, J.-F. (2014). Can regional climate engineering save the summer Arctic sea ice? *Geophys Research Letters*, *41*, 880–885. https://doi.org/10.1002/2013GL058731

Tilmes, S., Richter, J. H., Mills, M. J., Kravitz, B., MacMartin, D. G., Vitt, F., … Lamarque, J.-F. (2017). Sensitivity of aerosol distribution and climate response to stratospheric SO_2 injection locations. *Journal of Geophysical Research: Atmospheres*, *122*. https://doi.org/10.1002/2017JD026888

Weisenstein, D. K., Penner, J. E., Herzog, M., & Liu, X. (2007). Global 2-D intercomparison of sectional and modal aerosol modules. *Atmospheric Chemistry and Physics*, *7*, 2339–2355. https://doi.org/10.5194/acp-7-2339-2007

Weisenstein, D. K., Keith, D. W., & Dykema, J. A. (2015). Solar geoengineering using solid aerosol in the stratosphere. *Atmospheric Chemistry and Physics*, *15*, 11,835–11,859. https://doi.org/10.5194/acp-15-11835-2015